Inorganic Chemistry

pubs.acs.org/IC Article

Mn^{2+} Complexes Containing Sulfonamide Groups with pH-Responsive Relaxivity

Rocío Uzal-Varela, Aurora Rodríguez-Rodríguez, Miguel Martínez-Calvo, Fabio Carniato, Daniela Lalli, David Esteban-Gómez, Isabel Brandariz, Paulo Pérez-Lourido, Mauro Botta,* and Carlos Platas-Iglesias*

Cite This: https://dx.doi.org/10.1021/acs.inorgchem.0c02098 Read Online

ACCESS | Metrics & More | Article Recommendations | Supporting Information

ABSTRACT: We present two ligands containing a *N*-ethyl-4-(trifluoromethyl)-benzenesulfonamide group attached to either a 6,6′-(azanediylbis(methylene))-dipicolinic acid unit (H_3DPASAm) or a 2,2′-(1,4,7-triazonane-1,4-diyl)diacetic acid macrocyclic platform (H_3NO2ASAm). These ligands were designed to provide a pH-dependent relaxivity response upon complexation with Mn^{2+} in aqueous solution. The protonation constants of the ligands and the stability constants of the Mn^{2+} complexes were determined using potentiometric titrations complemented by spectrophotometric experiments. The deprotonations of the sulfonamide groups of the ligands are characterized by protonation constants of log K_i^H = 10.36 and 10.59 for $DPASAm^{3-}$ and $HNO2ASAm^{2-}$, respectively. These values decrease dramatically to log K_i^H = 6.43 and 5.42 in the presence of Mn^{2+}, because of the coordination of the negatively charged sulfonamide groups to the metal ion. The higher log K_i^H value in $[Mn(DPASAm)]^-$ is related to the formation of a seven-coordinate complex, while the metal ion in $[Mn(NO2ASAm)]^-$ is six-coordinated. The X-ray crystal structure of $Na[Mn(DPASAm)(H_2O)]\cdot 2H_2O$ confirms the formation of a seven-coordinate complex, where the coordination environment is fulfilled by the donor atoms of the two picolinate groups, the amine N atom, the N atom of the sulfonamide group, and a coordinated water molecule. The lower conditional stability of the $[Mn(NO2ASAm)]^-$ complex and the lower protonation constant of the sulfonamide group results in complex dissociation at relatively high pH (<7.0). However, protonation of the sulfonamide group in $[Mn(DPASAm)]^-$ falls into the physiologically relevant pH window and causes a significant increase in relaxivity from r_{1p} = 3.8 mM^{-1} s^{-1} at pH 9.0 to r_{1p} = 8.9 mM^{-1} s^{-1} at pH 4.0 (10 MHz, 25 °C).

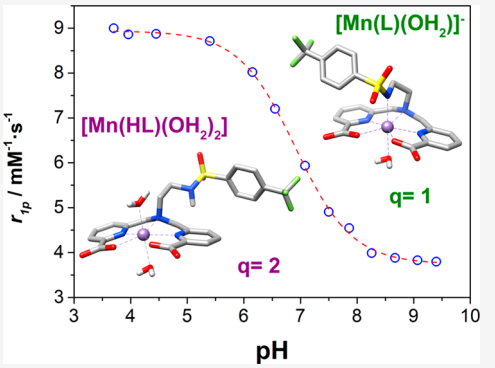

INTRODUCTION

Contrast agents for application in magnetic resonance imaging (MRI) are a class of paramagnetic compounds that are injected in the body to enhance image contrast, thereby aiding a more precise and accurate diagnosis of different pathologies.[1,2] Paramagnetic ions containing Mn^{2+} and Fe^{3+} were considered as MRI agents in the early times of MRI, back in the 1970s and early 1980s.[3−6] Soon afterward, it was discovered that some Gd^{3+} complexes are very efficient relaxation agents,[7] which were subsequently introduced in clinical practice and applied to aid diagnosis in millions of MRI scans every year.[1] Contrast agents based on Gd^{3+} are complexes with polyaminopolycarboxylate ligands that ensure a very high stability to avoid the release of the toxic metal ion in vivo.[8] These complexes contain a water molecule coordinated to the metal ion that exchanges with the water of the surrounding tissues, providing an efficient mechanism to shorten the relaxation times of water proton nuclei, thereby increasing the signal intensity.[9]

The contrast agents available in the market are considered very safe pharmaceuticals, although some problems of toxicity have been reported. These toxicity issues have been associated with the administration of Gd^{3+} agents to patients having renal impairment, which accumulate the metal ion in the body and, in some cases, develop a potentially fatal disease called nephrogenic systemic fibrosis.[10,11] This prompted the different medicine agencies to revise some of the protocols and prescribe information warnings, which prevented the detection of new cases. More recently, reports of Gd^{3+} deposition in the brain and other organs opened the debate on the long-term safety of some Gd^{3+} contrast agents,[12] which eventually led to the suspension of the authorizations in Europe of some of the agents based on nonmacrocyclic structures.[13]

The past decade witnessed a renewed interest in developing transition-based MRI probes as alternatives to the classical Gd^{3+} agents.[14,15] In particular, both Mn^{2+} and Fe^{3+} complexes were proposed as Gd^{3+} alternatives as T_1-shortening contrast agents, since they can reach relaxivities comparable to those of

Received: July 15, 2020

https://dx.doi.org/10.1021/acs.inorgchem.0c02098
Inorg. Chem. XXXX, XXX, XXX−XXX

commercially available Gd^{3+} agents.[16,17] These two metal ions present ^6S ground-energy terms for the free ion, that often originate ground-energy electronic states characterized by slow relaxation times of the electron spin in high-spin complexes, making them powerful relaxation agents. As in the case of Gd^{3+} agents,[18−20] responsive contrast agents may be designed by programming a change in the number of coordinated water molecules triggered by an alteration of a physiologically relevant parameter (i.e., pH, concentration of biogenic anions or cations). This was demonstrated recently by Tircsó et al. with the [Mn(PC2A-EA)] complex (Chart 1). The aminoethyl group of the ligand is protonated in the biologically relevant pH window (log K^{H}_{MnL} = 6.88), so that a water molecule replaces the amine donor atom, causing a remarkable relaxivity increase.[21]

Chart 1. Ligands Discussed in the Present Work

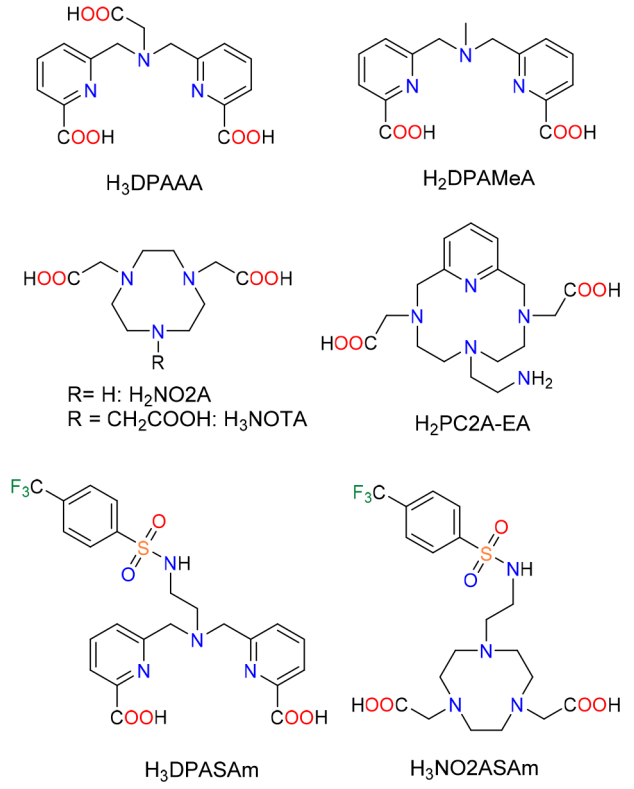

A few years ago, we initiated a research program aimed at developing potential candidates as Mn^{2+}-based MRI contrast agents. We developed a series of ligands based on both macrocyclic and acyclic frameworks, functionalized with picolinate or acetate pendant arms. Some representative members of the picolinate family are H_3DPAAA, H_2DPAMeA, and their derivatives (see Chart 1).[22,23] Among the macrocyclic ligands, we explored derivatives of 1,4,7-tetraazacyclononate,[24] containing two acetate groups (H_2NO2A) incorporating different functions on the third N atom of the macrocyclic unit,[25] or cyclen-based ligands such as H_2DO2A and related systems.[26] The Mn^{2+} complexes of $DPAAA^{3-}$ and $NO2A^{2-}$ were shown to contain a water molecule coordinated to the metal ion; DPAMeA yields a Mn^{2+} complex with two inner-sphere water molecules.

The *N*-ethylbenzenesulfonamide group was found to be well-suited to provide Gd^{3+}-based agents with pH-dependent modulation of ^1H relaxivity.[27] Thus, we hypothesized that the incorporation of an *N*-ethylbenzenesulfonamide group to these platforms should provide rather stable Mn^{2+} complexes with pH-responsiveness, since the deprotonated sulfonamide group is expected to remain coordinated to the metal ion. Sulfonamide protonation should trigger the coordination of a water molecule replacing the sulfonamide N atom, resulting in an increase of proton relaxivity and, thus, MRI contrast.

Herein, we present the synthesis and characterization of the ligands containing *N*-ethyl-4-(trifluoromethyl)-benzenesulfonamide groups H_3DPASAm and H_3NO2ASAm (see Chart 1). The presence of the electron-withdrawing CF_3 group was envisaged to push the pK_a of the sulfonamide group to the biologically relevant window, in view of the lower charge of Mn^{2+}, compared to Gd^{3+}. We report the synthesis of the ligands, a detailed assessment of the thermodynamic stability of the corresponding Mn^{2+} complexes, and their relaxometric behavior. We also present the X-ray structure of the $[Mn(H_3DPASAm)]^-$ complex.

RESULTS AND DISCUSSION

Synthesis. The H_3DPASAm ligand was synthesized by alkylation of *N*-(2-aminoethyl)-4-(trifluoromethyl)-benzenesulfonamide (**1**) with ethyl 6-(chloromethyl)picolinate and subsequent acid hydrolysis of the ester groups (see Scheme 1). Compound **1** was obtained in 92% by reaction of 4-(trifluoromethyl)benzenesulfonyl chloride and ethylendiamine in CH_2Cl_2 at 0 °C. The ligand was isolated with an overall yield of 36% over the three steps. Ligand H_3NO2ASAm was prepared by alkylation of the $NO2A(O^tBu)_2$ precursor with *N*-(2-bromoethyl)-4-(trifluoromethyl)-benzenesulfonamide (**3**) in acetonitrile in the presence of K_2CO_3 as a base (Scheme 1). The latter was isolated in 81% yield by reaction of 2-bromoethan-1-amine hydrobromide and 4-(trifluoromethyl)benzenesulfonyl chloride, using Et_3N as a base. Acid hydrolysis of the *tert*-butyl ester groups of the ester intermediate **4** with 3 M HCl at room temperature afforded the desired ligand in 71% yield over the three steps.

X-ray Structure. Single crystals with a formula of $Na[Mn(DPASAm)(H_2O)]\cdot 2H_2O$ were obtained by slow evaporation of an aqueous solution of the complex at pH 9.9. Crystals contain two $[Mn(DPASAm)(H_2O)]^-$ complexes joined by two Na^+ cations, generating a centrosymmetric $\{Na_2(H_2O)_2[Mn(DPASAm)(H_2O)]_2\}$ entity (Figure 1). Table 1 presents the bond distances of the metal coordination environments. Each Mn^{2+} ion is coordinated to the tertiary N atom of the ligand N2 and the donor atoms of the picolinate groups N1, N3, O1, and O3, which define a pentagonal plane of the pentagonal bipyramidal coordination polyhedron (deviation from planarity = 0.19 Å). Heptacoordination is relatively rare in first-row transition-metal complexes, being however more common for Mn than for any other element of the series.[28] The N atom of the sulfonamide group N4 and the oxygen atom of a coordinated water molecule O7 occupy the apical positions of the pentagonal bipyramid. The N4−Mn1−O7 angle (174.76(8)°) deviates by ∼5° from the linear value expected for a pentagonal bipyramid. The angles defined by adjacent donor atoms of the equatorial plane and the metal ion fall within the range of 68.8°−79.3°, and thus present relatively small deviations from the ideal value (72°).

The sulfonamide N atom N4 gives the strongest interaction with the Mn^{2+} ion, while the tertiary amine N atom N2 appears to provide a rather weak bond, as usually observed in

https://dx.doi.org/10.1021/acs.inorgchem.0c02098
Inorg. Chem. XXXX, XXX, XXX−XXX

Scheme 1. Synthesis of the H_3DPASAm and H_3NO2ASAm Ligands

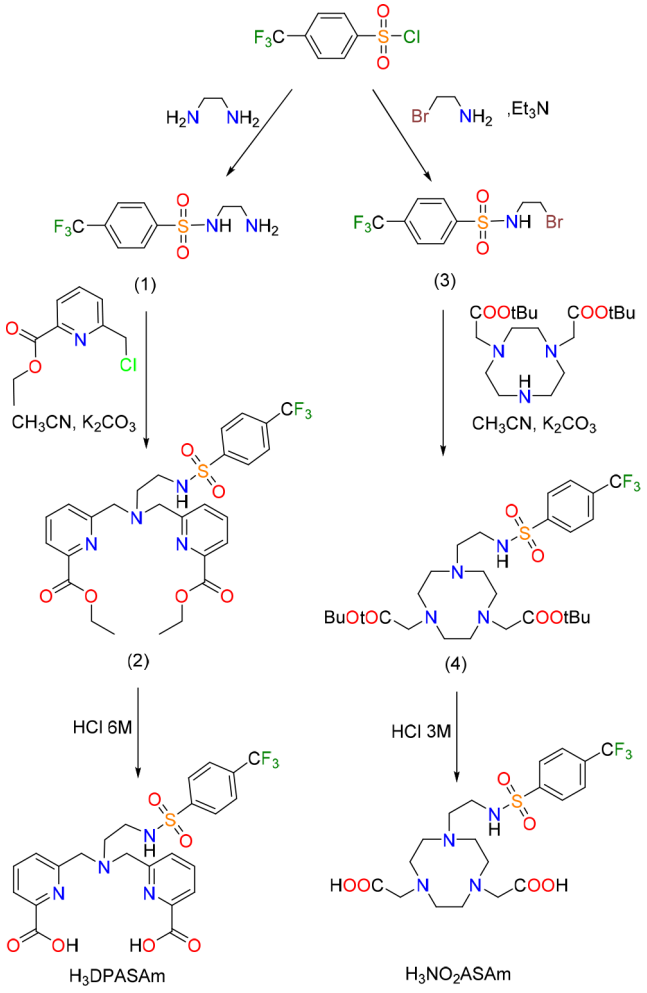

complexes with tripodal ligands.[29] The bond distances involving the donor atoms of the picolinate groups are similar to those reported for related seven-coordinate Mn^{2+} complexes.[24,29] The sulfonamide group is a relatively common motif in Mn^{2+} coordination chemistry that is generally coordinated through the N atom.[30]

The Na^+ cations are coordinated to an oxygen atom of the sulfonamide group (O6) and three oxygen atoms of the carboxylate groups (O1, O3, and O4). The carboxylate group containing O1 and O4 is involved in μ^3-η^1:η^2 coordination through O1 and O4, while the carboxylate group containing O3 provides a μ^2-η^2 coordination.[31] Six-coordination is completed by the O atoms of two water molecules, resulting in a distorted octahedral environment around the Na^+ cations. The Mn−O distance involving the μ^2-η^2 carboxylate (Mn−O3 = 2.2188(15) Å) is ca. 0.05 Å shorter than the Mn−O1 bond (2.2600(15) Å), which implies a μ^3-η^1:η^2 carboxylate.

Ligand Protonation Constants and Stability Constants of the Mn^{2+} Complexes. The protonation constants of the NO2ASAm^{3-} ligand were determined by potentiometric titrations at 25 °C in 0.15 M NaCl. However, potentiometry did not allow an accurate determination of the values of log K_1^H and log K_2^H, likely because of partial (nonvisible) precipitation of the ligand. Thus, both potentiometric and spectrophotometric titrations were used for independent protonation constant determination. Representative potentiometric titrations curves are presented in Figures S1 and S2 in the Supporting Information. The protonation constants of DPASAm^{3-} were determined using spectrophotometric titrations, because precipitation was observed at the concentration required for potentiometric experiments (>1 mM). Table 2 compares the determined log K_i^H values with those reported for the analogous ligands containing an acetate group replacing the sulfonamide pendant (DPAAA^{3-} and NOTA^{3-}).[22,32,33] The data reported in the literature for NOTA^{3-} was measured using 0.1 M ionic strengths, and thus we used potentiometry to determine the protonation constants of this ligand, using a 0.15 M NaCl background electrolyte.

The absorption spectrum of DPASAm^{3-} recorded at pH 0.82 is dominated by a band with a maximum at 269 nm, characteristic of the picolinic acid chromophore (see Figure 2).[34] Increasing the pH causes an increase in the intensity of the absorption maximum, which experiences a slight shift to longer wavelengths. The absorption spectra recorded in the pH range of 0.82−12.45 were fitted to obtain the ligand

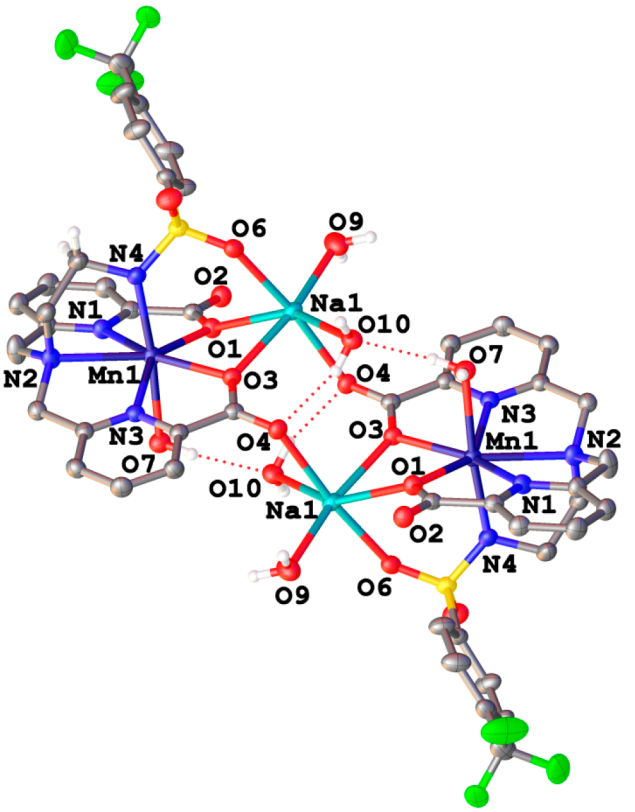

Figure 1. X-ray crystal structure of Na[Mn(DPASAm)(H_2O)]·2H_2O with atom numbering. The ORTEP plot is at the 50% probability level.

Table 1. Bond Distances of the Metal Coordination Environments in Na[Mn(DPASAm)(H_2O)]·2H_2O

bond	bond distance (Å)	bond	bond distance (Å)
Mn1−N4	2.197(2)	Na1−O1	2.5295(18)
Mn1−O3	2.2188(15)	Na1−O3	2.3951(17)
Mn1−O1	2.2600(15)	Na1−O4	2.4741(18)
Mn1−N1	2.2609(19)	Na1−O6	2.3484(18)
Mn1−N3	2.2716(18)	Na1−O9	2.381(2)
Mn1−O7	2.3457(16)	Na1−O10	2.5160(18)
Mn1−N2	2.514(2)		

https://dx.doi.org/10.1021/acs.inorgchem.0c02098
Inorg. Chem. XXXX, XXX, XXX−XXX

Table 2. Protonation Constants of the Ligands and Stability Constants of Their Mn^{2+} Complexes Determined by Potentiometric and Spectrophotometric Titrations at 25 °C in 0.15 M NaCl

	$DPASAm^{3-}$[a]	$DPAAA^{3-}$[b]	$NO2ASAm^{3-}$	$NOTA^{3-}$ (I = 0.15 M)	$NOTA^{3-}$ (I = 0.1 M)
log K_1^H	10.36(1)	7.26	11.26(7)[a]	12.05(6)	13.17[c]/11.41[d]
log K_2^H	6.13(1)	3.90	10.59(8)[a]	5.77(6)	5.74[c]/5.74[d]
log K_3^H	3.68(1)	3.29	4.57(5)/4.57(5)[a]	3.30(6)	3.22[c]/3.16[d]
log K_4^H	2.43(1)	1.77	2.65(5)/2.69(5)[a]	2.20(7)	1.96[c]/1.71[d]
log K_{MnL}	13.53(1)	13.19	15.29(5)	15.6(1)	16.30[c]/14.9[e]
log K_{MnLH}	6.44(2)	2.90	5.52(5)		
log K_{MnLOH}	–	11.97			
pMn[f]	7.82	8.98	6.63	7.97	

[a]Values obtained with spectrophotometric titrations at 25 °C in 0.15 M NaCl. [b]Equilibrium constants in 0.15 M NaCl and 25 °C taken from ref 22. [c]Equilibrium constants in 0.1 M Me_4NCl ionic strength and 25 °C taken from ref 32. [d]Equilibrium constants in 0.1 M ionic strength and 25 °C taken from ref 33. [e]Stability constant in 0.1 M Me_4NCl ionic strength and 25 °C taken from ref 39. [f]Defined as $-\log[Mn^{2+}]_{free}$ at pH 7.4 for $[Mn^{2+}]_{tot} = [L]_{tot} = 10^{-5}$ M.

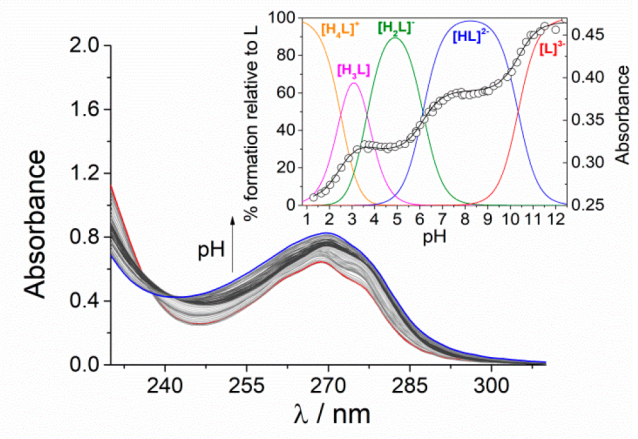

Figure 2. Absorption spectra of a 6.55×10^{-5} M solution of $DPASAm^{3-}$ recorded at different pH values (blue trace, pH 12.45; red trace, pH 0.82). Inset shows changes in absorbance at 249 nm (circles), fitted values (black line), and the species distribution diagram.

protonation constants listed in Table 2. The absorption spectra calculated for the different species present in solution are shown in Figure S3 in the Supporting Information.

The first protonation constant of the $DPASAm^{3-}$ ligand ($\log K_1^H$ = 10.36) can be assigned to the protonation of the sulfonamide N atom by comparison with the protonation constants of $DPAAA^{3-}$. This protonation constant is similar to that reported for DO3A ligands containing sulfonamide (log K^H = 11.02)[35] or dansyl (log K^H = 10.8)[36] groups. The second protonation event involves the amine N atom of the ligand, while log K_3^H and log K_4^H are associated with the protonation of the carboxylate functions of the picolinate groups.[37]

The $NO2ASAm^{3-}$ ligand presents two protonation constants with log K_i^H values of 11.26 and 10.59, which are related to the protonation of the sulfonamide group and a N atom of the macrocyclic fragment. However, an unambiguous attribution of each protonation event is not possible, based on potentiometric data. Therefore, we performed spectrophotometric titrations in the pH range of ca. 9–13. The absorption spectrum of the ligand recorded at pH ~9 presents a well-defined maximum at 268 nm, with two additional components at 262 and 276 nm (see Figure S4 in the Supporting Information), typical of the sulfonamide chromophore.[38] The increase in the pH of the solution provokes an increase of the intensity of the band, which becomes broader and ill-defined. The absorption band experiences drastic changes above pH ~9, associated with a protonation constant of log K_2^H = 10.59(8). However, the protonation event associated with a protonation constant of log K_1^H = 11.26(7) is characterized by slight changes of the absorption spectrum. Thus, the first protonation constant of $NO2ASAm^{3-}$ can be attributed to the macrocyclic ring, while the second is assigned to the sulfonamide group. Therefore, the sulfonamide groups in $DPASAm^{3-}$ and $NO2ASAm^{3-}$ are characterized by very similar protonation constants. Spectrophotometric titrations of $NO2ASAm^{3-}$ in the pH range of 1.6–6.2 were also performed (see Figure S5 in the Supporting Information). Although spectral variations were not as pronounced as at basic pH, the protonation constants LogK_3^H and log K_4^H obtained by this method show an excellent agreement with the potentiometric data (see Table 2).

A comparison of the protonation constants associated with the amine N atom of $DPAAA^{3-}$ (log K_1^H = 7.26) and $DPASAm^{3-}$ (log K_2^H = 6.13) shows that the substitution of the acetate group by an *N*-ethylsulfonamide pendant causes a decrease in the basicity of the amine N atom. A similar effect is evident by comparing the log K_1^H values determined for $NO2ASAm^{3-}$ and $NOTA^{3-}$.

The first protonation constant determined for $NOTA^{3-}$ in 0.15 M NaCl is ca. 1 log K unit lower than that measured in 0.1 M Me_4NCl,[32] which likely reflects the formation of a relatively stable Na^+ complex. The remaining protonation constants determined using these two ionic strength backgrounds are in excellent agreement. Speciation diagrams calculated for $DPASAm^{3-}$, $NO2ASAm^{3-}$ and $NOTA^{3-}$ are presented in Figures S6–S8 in the Supporting Information.

The stability constants of the Mn^{2+} complexes were determined using spectrophotometric ($DPASAm^{3-}$) or potentiometric ($NO2ASAm^{3-}$ and $NOTA^{3-}$) titrations. The absorption spectra of the Mn^{2+}:$DPASAm^{3-}$ system experience important changes with pH (see Figure 3). The intensity of the absorption maximum at 269 nm decreases in the pH range of 1.3–3.4 as the protonated complex [Mn(HDPASAm)] is formed. The deprotonation and coordination of the sulfonamide pendant induces a second decrease of the absorbance at 269 nm above pH ~4.5 until reaching pH ~7.8.

The stability of the $NOTA^{3-}$ complex was also investigated using potentiometry, for comparative purposes. The stability constant of the Mn^{2+} complexes with $NOTA^{3-}$ determined in 0.15 M NaCl (log K_{MnL} = 15.6) is slightly lower than that reported in 0.1 M Me_4NCl (log K_{MnL} = 16.3). These values, in

https://dx.doi.org/10.1021/acs.inorgchem.0c02098
Inorg. Chem. XXXX, XXX, XXX–XXX

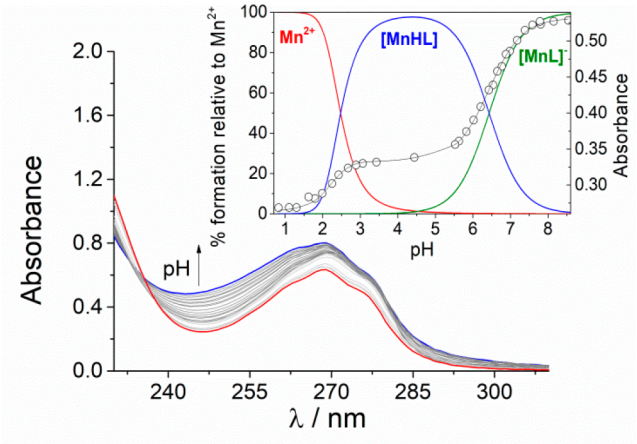

Figure 3. Absorption spectra of a 6.55 × 10^{-5} M solution of $DPASAm^{3-}$ and 1 equiv of Mn^{2+} recorded at different pH values (blue trace, pH 8.54; red trace, pH 0.82). Inset shows changes in absorbance at 250 nm (circles) and species distribution diagram.

turn, are slightly higher than those reported initially by Sherry et al. in 0.1 M Me_4NCl (log K_{MnL} = 14.9).[39]

The stability constants determined for the Mn^{2+} complexes of $DPASAm^{3-}$ and $NO2ASAm^{3-}$ are comparable to those of the parent carboxylate analogues $DPAAA^{3-}$ and $NOTA^{3-}$. However, the high basicity of the sulfonamide group provokes a significant decrease of the conditional stability at physiologically relevant pH values. This is reflected in the calculated pMn values, which define the stability of the complexes under specific conditions.[40] The pMn value determined for the $NO2ASAm^{3-}$ complex is one unit lower than that of $DPAAA^{3-}$, with an even more pronounced effect observed by comparing the pMn values of the $NO2ASAm^{3-}$ and $NOTA^{3-}$ complexes. The lower basicity of $DPAAA^{3-}$ is also responsible for the high pMn value, compared to $NOTA^{3-}$, despite the fact that the log K_{MnL} value is more than 2 orders of magnitude higher for the latter.

Both the $[Mn(DPASAm)]^-$ and $[Mn(NO2ASAm)]^-$ complexes protonate at relatively high pH values, with log K_{MnHL} values of 6.43 and 5.52, respectively. These protonation events can be ascribed to the protonation of the sulfonamide group. The decrease of 4−5 orders of magnitude in the protonation constants of the sulfonamides in the presence of Mn^{2+} confirms the coordination of the sulfonamide N atom to the metal ion, as observed in the solid state (see above). The coordinated sulfonamide group is more basic in $[Mn(DPASAm)]^-$ than in $[Mn(NO2ASAm)]^-$. This likely reflects a stronger coordination of the sulfonamide N atom in the six-coordinate $[Mn(NO2ASAm)]^-$ complex, compared to the seven-coordinate $[Mn(DPASAm)]^-$ analogue.

The speciation diagrams calculated for the Mn^{2+}:$DPASAm^{3-}$ and Mn^{2+}:$NO2ASAm^{3-}$ systems, using the equilibrium constants given in Table 2, clearly confirm the higher stability of the $[Mn(DPASAm)]^-$ complex, which protonates below pH ∼9 and exists largely as the protonated form in the pH range of 5−4 (see Figure 4). Below pH ∼4, complex dissociation occurs. Conversely, $[Mn(NO2ASAm)]^-$ protonates at a lower pH (less than ∼8.0), already dissociating below pH 7.0. As a result, the maximum concentration of the protonated species is observed at pH 5.1 (55%), with 18% and 27% of the total manganese being present as the anionic complex and the free metal ion, respectively. The $[Mn(NOTA)]^-$ complex dissociates below pH ∼5 (see Figure S9 in the Supporting Information).

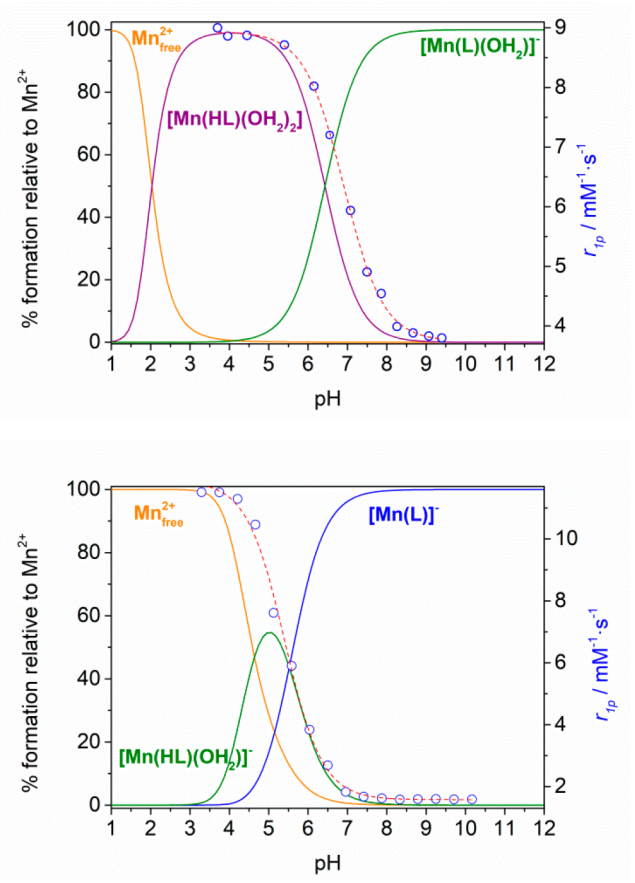

Figure 4. Speciation diagrams calculated for the Mn^{2+}:$DPASAm^{3-}$ (top) and Mn^{2+}:$NO2ASAm^{3-}$ (bottom) systems. $[Mn^{2+}]$ = [L] = 10^{-3} M. Circles represent the relaxivities of $[Mn(DPASAm)]^-$ (top) and $[Mn(NO2ASAm)]^-$ (bottom) recorded at different pH values (298 K, 10 MHz).

Relaxometric Study. The potential response of $[Mn(DPASAm)]^-$ and $[Mn(NO2ASAm)]^-$ to changes in pH was analyzed by measuring proton relaxivities (r_{1p}) of aqueous solutions of the complexes at 10 MHz and 25 °C. The $[Mn(NO2ASAm)]^-$ complex presents a low and constant relaxivity of 1.6 mM^{-1} s^{-1} in the pH range of 7−10 (see Figure 4). This relaxivity is characteristic of Mn^{2+} complexes that lack coordinated water molecules (q = 0), the observed relaxivity being the result of the outer-sphere contribution.[41] The outer-sphere contribution is the result of the dipolar coupling between the electron spin of the paramagnetic center and the nuclear spins of water molecules diffusing in the proximity of the paramagnetic complex. Lowering the pH below pH 7 results in a sharp increase of r_{1p}, which reaches a value of 11.5 mM^{-1} s^{-1} at pH 2.5. This agrees with the species distribution diagram reported in Figure 4, which shows that protonation of the complex occurs below pH ∼8 and complex dissociation below pH ∼7. Thus, the increase in relaxivity observed below pH ∼7 is likely related to both complex protonation and dissociation. To confirm this, we recorded ^{1}H nuclear magnetic relaxation dispersion (NMRD) profiles at pH 4.0. The NMRD profile shows the dispersion in the range of 3−20 MHz, typical of small Mn^{2+} complexes, together with a second dispersion below 1 MHz that is characteristic of the scalar contribution to

https://dx.doi.org/10.1021/acs.inorgchem.0c02098
Inorg. Chem. XXXX, XXX, XXX−XXX

relaxivity in the aquated $[Mn(H_2O)_6]^{2+}$ complex (see Figure 5, as well as Figure S10 in the Supporting Information).[42,43] This

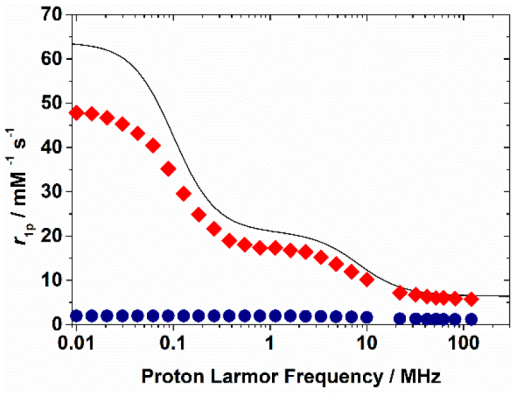

Figure 5. Comparison between the ^{1}H NMRD profile of [Mn(NO2ASAm)]$^-$ recorded at pH 8.0 (blue circles), pH 4.0 (red diamonds), and the ^{1}H NMRD profile of $[Mn(H_2O)_6]^{2+}$ reported in ref 42. All data were acquired at 298 K.

indicates that, at pH 4, the complex is largely dissociated, which is consistent with the speciation diagram shown in Figure 4.

The relaxivity of the [Mn(NO2ASAm)]$^-$ complex was further analyzed by recording ^{1}H NMRD profiles at pH 8.0 and three different temperatures (283, 298, and 310 K) in the

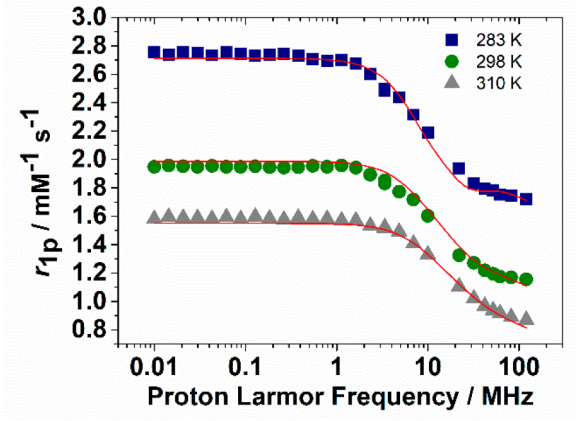

Figure 6. ^{1}H NMRD profiles of [Mn(NO2ASAm)]$^-$ recorded at pH 8.0. The solid lines correspond to the fit of the data as described in the text.

proton Larmor frequency range of 0.01−120 MHz (Figure 6). ^{1}H relaxivity decreases as the temperature increases, as expected, because of the increase of the relative translational diffusion coefficient D_{MnH}.[44] The relaxivities observed for [Mn(NO2ASAm)]$^-$ were analyzed using Freed's outer-sphere model.[45] The fits of the NMRD data were performed by assuming a value of 3.6 Å for a_{MnH}, which is the distance of closest approach of the proton nuclei of outer sphere water molecules to the paramagnetic ion. All other parameters were determined from the least-squares fit of the data (see Table 3).

The values of the relative diffusion coefficient (D^{298}_{MnH}) and its activation energy (E_{DMnH}) are very similar to those determined for the self-diffusion of water in water (23×10^{-10} m^2 s^{-1} and 17.6 kJ mol^{-1}, respectively).[46] This is expected, as D^{298}_{MnH} is the sum of the self-diffusion coefficients of water molecules and the paramagnetic species, and water diffuses much faster than the complex. Thus, these parameters support the reliability of the analysis, indicating that the value assumed for a_{MnH} is reasonable.

The relaxivity of the DPASAm^{3-} complex at pH 9 (10 MHz, 25 °C, 3.8 mM^{-1} s^{-1}) is compatible with the presence of a water molecule in the first coordination sphere of the metal ion. Decreasing the pH of the solution causes an important increase in relaxivity, which reaches a value of 8.9 mM^{-1} s^{-1} in the pH range of 5.5−4.0 (Figure 4). This behavior can be attributed to the protonation and decoordination of the sulfonamide group, which allows a second water molecule to enter the Mn^{2+} coordination environment, yielding a bis-hydrated complex at low pH. The analysis of the r_{1p} vs pH dependence yields a pK_a of 6.90 ± 0.02. This value differs slightly from that obtained with potentiometric measurements (pK_a = 6.43; recall Table 2), likely as a result of the different ionic strengths used in the two experiments.

The ^{1}H NMRD profiles of the DPASAm^{3-} complex were recorded at three temperatures and pH values of 9.1 and 4.7 (see Figure 7), so that the nonprotonated [Mn(DPASAm)]$^-$ and the protonated [Mn(HDPASAm)] species are largely dominant (recall Figure 4). The relaxivities observed at low pH are higher than those determined at basic pH over the entire range of proton Larmor frequencies, which is consistent with an increased hydration number upon complex protonation.

The inner-sphere contribution to relaxivity ($r_{1p,is}$) in Mn^{2+} complexes is dependent on the relaxation rate of inner sphere protons (T^H_{1m}), the mean residence time of a water molecule in the inner coordination sphere of the metal ion ($\tau_m = 1/k_{ex}$), and the number of inner-sphere water molecules (q):[47]

$$r_{1p,is} = \frac{1}{1000} \times \frac{q}{55.55} \times \frac{1}{T^H_{1m} + \tau_m} \quad (1)$$

The relaxation rate of inner sphere protons in Mn^{2+} complexes other than the aqua ion is generally dominated by the dipole−dipole (DD) mechanism:[48]

$$\left(\frac{1}{T^H_{1m}}\right)^{DD} = \frac{2}{15}\left(\frac{\mu_0}{4\pi}\right)^2 \frac{\gamma_I^2 g^2 \mu_B^2}{r_{MnH}^6} S(S+1)\left(\frac{3\tau_{d1}}{1+\omega_I^2\tau_{d1}^2} + \frac{7\tau_{d2}}{1+4\omega_s^2\tau_{d2}^2}\right) \quad (2)$$

In eq 2, g is the electron g-factor, r_{MnH} the distance between the electron and nuclear spins, μ_B the Bohr magneton, γ_I the ^{1}H gyromagnetic ratio, S the total spin (5/2 for a high-spin Mn^{2+} complex), ω_I the proton resonance frequency, and ω_S the Larmor frequency of the Mn^{2+} electron spin. The correlation time τ_{di} is given by eq 3, where τ_R is the rotational correlation time, and T_{ie} are the longitudinal (i = 1) and transverse (i = 2) relaxation times of the electron spin.

$$\frac{1}{\tau_{di}} = \frac{1}{\tau_R} + \frac{1}{\tau_m} + \frac{1}{T_{ie}} \qquad \text{with } i = 1, 2 \quad (3)$$

The τ_R values characteristic of small Mn^{2+} complexes are typically <100 ps, while τ_m is generally in the nanosecond time scale. Furthermore, most often, T^H_{1m} is longer than τ_m, so that water exchange has little effect in eq 1. As a result, ^{1}H NMRD profiles are quite often insensitive to water exchange. Unfortunately, the low solubility of the DPASAm^{3-} complex prevented us from recording ^{17}O NMR measurements, which provide direct access to water exchange dynamics.[49]

https://dx.doi.org/10.1021/acs.inorgchem.0c02098
Inorg. Chem. XXXX, XXX, XXX−XXX

Table 3. Parameters Obtained from the Fits of ^{1}H NMRD Data

parameter	Value				
	[Mn(HDPASAm)]	[Mn(DPASAm)]$^-$	[Mn(NO2ASAm)]$^-$	[Mn(DPAMeA)][b]	[Mn(DPAAA)]$^-$[c]
k_{ex}^{298} ($\times 10^7$ s^{-1})	30.6[a]	–	–	30.6	12.6
$\Delta H^{\ddagger}$ (kJ mol^{-1})	28.1[a]	–	–	28.1	42.7
τ_R^{298} (ps)	72.0 ± 0.8	99.4 ± 4.4	–	47.8	47.6
E_r (kJ mol^{-1})	23.9 ± 0.5	21.6 ± 1.8	–	25.3	22.8
τ_v^{298} (ps)	56 ± 2	14.3 ± 0.06	15.6 ± 0.9	39.2	19.4
D_{MnH}^{298} ($\times 10^{-10}$ m^2 s^{-1})	22.3[a]	22.3[a]	22.3 ± 0.2	22.4	22.4
E_{DMnH} (kJ mol^{-1})	23[a]	23[a]	23 ± 5	17.3	17.3
Δ^2 ($\times 10^{20}$ s^{-2})	0.130 ± 0.010	0.76 ± 0.05	1.7 ± 0.1	0.238	0.55
r_{MnH} (Å)	2.741[a]	2.741[a]	–	2.74	2.756[a]
a_{MnH} (Å)	3.6[a]	3.6[a]	3.6[a]	3.6	3.6[a]
q^{298}	2[a]	1[a]	0[a]	2	1[a]

[a]Parameters fixed during the fitting procedure. [b]Data from ref 23. [c]Data from ref 22.

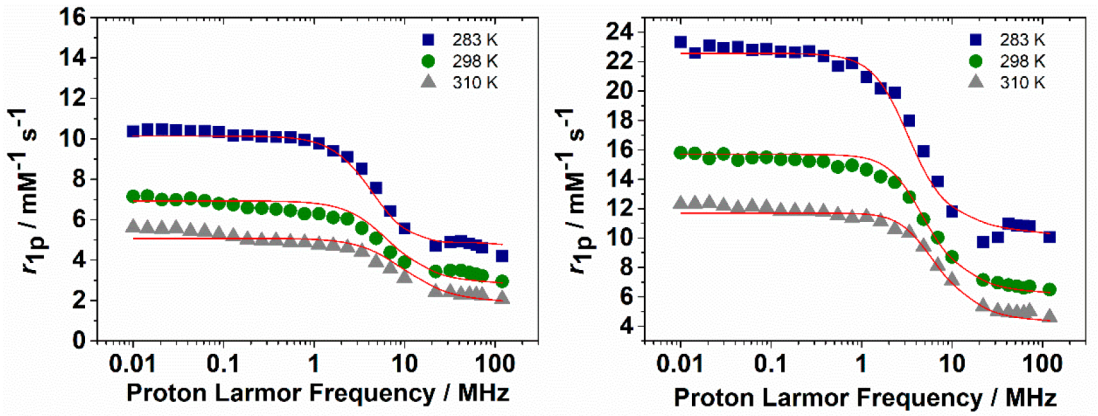

Figure 7. ^{1}H NMRD profiles of the Mn^{2+} complex of $DPASAm^{3-}$ recorded at pH 9.1 (left) and 4.7 (right). The solid lines correspond to the fit of the data, as described in the text.

The ^{1}H NMRD profiles recorded at basic pH, where the [Mn(DPASAm)]$^-$ species largely dominates the speciation in solution, could be fitted very well by assuming that τ_m provides a negligible contribution to eqs 1 and 3 (recall Table 3 and Figure 7). Furthermore, we also fitted the temperature dependence of r_{1p} recorded at 32 MHz in the temperature range of 283−323 K (see Figure S11 in the Supporting Information). The fit of the data was performed by fixing some of the parameters to reasonable values: the diffusion coefficient and its activation energy were fixed to the values obtained for [Mn(NO2ASAm)]$^-$, a_{MnH} was set to 3.6 Å, the number of coordinated water molecules was assumed to be q = 1, and r_{MnH} was fixed to the average Mn···H_{water} distance observed in the X-ray structure of the complex described above. The fit of the data provided a τ_R^{298} value that is very reasonable (99 ps), considering the size of the complex.[23] The parameters characterizing the relaxation of the electron spin, the mean square transient ZFS energy (Δ^2), and its correlation time (τ_v) take values that are in the normal range observed for Mn^{2+} complexes.

The ^{1}H NMRD profiles recorded at pH 4.7, where the protonated [Mn(HDPASAm)] complex is the dominant species, together with the temperature dependence of r_{1p} at 32 MHz, were also analyzed quantitatively. Attempts to fit the data using the same approach applied for the data at high pH did not reproduce the experimental data well, particularly at low temperatures. This suggests that the contribution of τ_m to eq 3 is not negligible. In the absence of ^{17}O NMR data, because of solubility limitations, we hypothesized that the [Mn(HDPASAm)] complex must present a water exchange rate very similar to [Mn(DPAMeA)], as the two species are expected to present very similar coordination environments: a pentagonal bipyramidal coordination, where the equatorial plane is defined by the amine N atom and the donor atoms of the two picolinate units, with two water molecules occupying the axial positions.[23]

A very good fit of the experimental data was obtained by fixing k_{ex}^{298} and $\Delta H^{\ddagger}$ to the values determined for [Mn(DPAMeA)] from ^{17}O NMR measurements (recall Table 3).[23] This analysis yielded a τ_R^{298} value (72 ps) that is somewhat shorter than at basic pH, likely because of increased flexibility of the complex upon decoordination of the sulfonamide pendant.

The value of Δ^2 varies significantly, depending on the nature of the axial donor, being lower for the complex at low pH, where two water molecules occupy the axial positions. The ZFS energy is very sensitive to the symmetry of the coordination environment, increasing as the symmetry is lowered.[50] Thus, it is reasonable that the presence of two different donor atoms in axial positions (water and sulfonamide N atom) results in a higher ZFS energy. A similar trend can be observed by comparing the Δ^2 values reported for [Mn(DPAMeA)] and [Mn(DPAAA)]$^-$ (recall Table 3). In the latter case, a carboxylate oxygen atom occupies one of the axial positions in the pentagonal bipyramidal coordination environment.[22]

https://dx.doi.org/10.1021/acs.inorgchem.0c02098
Inorg. Chem. XXXX, XXX, XXX−XXX

CONCLUSIONS

In this work, we have presented two ligands containing a sulfonamide pendant and their Mn^{2+} complexes, which were conceived as potential pH-responsive MRI agents. In the case of $[Mn(DPASAm)]^-$, protonation of the sulfonamide group was observed close to the physiologically relevant pH range. Complex protonation provokes a 2.3-fold increase in ^1H relaxivity from r_{1p} = 3.8 mM^{-1} s^{-1} at pH 9.0 to r_{1p} = 8.9 mM^{-1} s^{-1} at pH 4.0 (20 MHz, 25 °C). Relaxometric and potentiometric studies are in good mutual agreement, showing that the complex is perfectly stable in the pH range of 4−10. The X-ray structure of the $[Mn(DPASAm)]^-$ complex evidences coordination of the deprotonated sulphonamide N atom, as well as the presence of a coordinated water molecule. The relaxometric characterization showed that the relaxivity increase observed upon complex protonation is related to the coordination of a second water molecule.

The $[Mn(NO2ASAm)]^-$ complex is also protonated, although the sulfonamide group was found to be considerably less basic than in $[Mn(DPASAm)]^-$ (pK_a = 5.5 and 6.4, respectively). This can be attributed to a stronger Mn−$N_{sulfonamide}$ interaction in $[Mn(NO2ASAm)]^-$, because of the lower coordination number of the metal ion. Besides the lower pK_a, $[Mn(NO2ASAm)]^-$ is characterized by a lower conditional stability than $[Mn(DPASAm)]^-$, associated with a high basicity of the macrocyclic structure. As a result, the $[Mn(NO2ASAm)]^-$ complex dissociates at a relatively high pH. These results highlight that ligand basicity plays a key role in the stability of potential Mn^{2+} MRI contrast agents, so that this issue should be carefully considered for ligand design. Overall, the results reported in this paper provide a proof-of-concept on the design of pH-responsive Mn^{2+} MRI probes based on reversible binding of sulfonamide groups, although further probe optimization to improve kinetic inertness is required for practical applications, as the $[Mn(DPASAm)]^-$ complex dissociates very quickly when challenged with an excess of Zn^{2+} (see Figure S35 in the Supporting Information). Another aspect that must be considered is the biodistribution of the probe, because the intensity of the MRI signal will be dependent both on the protonation state of the complex and the local concentration of the agent.

EXPERIMENTAL SECTION

Materials and Methods. Ethyl 6-(chloromethyl)picolinate[51] was prepared following the literature methods. Di-*tert*-butyl 2,2′-(1,4,7-triazonane-1,4-diyl)diacetate (NO2AtBu) was purchased from CheMatech (Dijon, France). All other reagents were purchased from Aldrich Chemical Co.

High-resolution electrospray-ionization time-of-flight ESI-TOF mass spectra were recorded using a LC-Q-q-TOF Applied Biosystems QSTAR Elite spectrometer in positive and negative mode. Mass spectra recorded using electron impact ionization were recorded with a Thermo MAT95XP instrument. Elemental analyses were accomplished on a ThermoQuest Flash EA 1112 elemental analyzer. Medium performance liquid chromatography (MPLC) was performed using a Puriflash XS 420 instrument equipped with a reverse-phase Puriflash 15C18HP column (60 Å, spherical 15 μm, 20 g) and UV-DAD detection at 210 and 254 nm, and operating at a flow rate of 10 mL/min. Aqueous solutions were lyophilized using a Telstar Cryodos-80 apparatus. ^1H, ^{13}C, and ^{19}F NMR spectra of the ligands and their precursors were recorded at 298 K, using Bruker AVANCE III 300 or Bruker Avance 500 spectrometers. ^{19}F chemical shifts were referenced by using sodium triflate on a D_2O solvent (δ 75.6 ppm).

***N*-(2-Aminoethyl)-4-(trifluoromethyl)benzenesulfonamide (1).** This compound was prepared using a slight modification of the synthesis reported in the literature.[52] A solution of 4-(trifluoromethyl)benzenesulfonyl chloride (0.500 g, 2.044 mmol) in CH_2Cl_2 (20 mL) was added to a solution of ethylendiamine (1.228 g, 20.43 mmol) in CH_2Cl_2 (200 mL) at 0 °C. The mixture was stirred at room temperature for 16 h and then extracted with 1 M HCl (3 × 100 mL). The combined aqueous phases were basified to pH 10 with NaOH and extracted with CH_2Cl_2 (3 × 100 mL). The organic extracts were dried with Na_2SO_4 and concentrated, affording **1** as a white solid (0.502 g, 1.871 mmol, 92% yield). ^1H NMR (300 MHz, $CDCl_3$) δ 8.01 (d, *J* = 8.2 Hz, 2H), 7.79 (d, *J* = 8.2 Hz, 2H), 3.00 (t, *J* = 5.6 Hz, 2H), 2.93−2.71 (m, 2H). ^{19}F NMR (282 MHz, $CDCl_3$) δ −63.1. MS (ESI^+): *m*/*z* calcd for $C_9H_{12}F_3N_2O_2S$ $[M + H]^+$: 269.06. Found: 269.06.

Diethyl 6,6′-(((2-((4-(trifluoromethyl)phenyl)sulfonamido)-ethyl)azanediyl)bis(methylene))dipicolinate (2). A solution of ethyl 6-(chloromethyl)picolinate (0.2981 g, 1.493 mmol) in dry CH_3CN (3 mL) was added dropwise to a solution of compound **1** (0.2001 g, 0.7459 mmol) containing K_2CO_3 (0.2577 g, 1.864 mmol) in dry CH_3CN (35 mL). A catalytic amount of KI was added and the mixture was purged with an argon flow while stirred at room temperature for 6 days. The reaction mixture was filtered and the filtrate was evaporated to dryness in vacuo. The product was purified by MPLC on neutral alumina (CH_2Cl_2:MeOH 90:10 (v:v)) and isolated as a yellow oil (0.2752 g, 0.4628 mmol, 62% yield). ^1H NMR (300 MHz, $CDCl_3$) δ 8.04 (m, 2H), 7.97 (m, 2H), 7.45−7.80 (m, 6H), 7.11 (b, 1H), 4.51 (q, ^3J = 7.1 Hz, 4H), 3.89 (s, 4H), 3.14 (b, 2H), 2.84 (m, 2H), 1.46 (t, ^3J = 7.1 Hz, 6H). ^{19}F NMR (282 MHz, $CDCl_3$) δ −63.0. ^{13}C NMR (75.5 MHz, $CDCl_3$) δ 165.0, 159.4, 147.6, 144.4, 137.4, 133.5 ($^1J_{C-F}$ = 32.2 Hz), 127.5, 126.3, 125.9, 123.5, 61.8, 59.5, 53.8, 41.3, 14.2. MS(ESI^+): *m*/*z* calcd for $C_{27}H_{29}F_3N_4NaO_6S$ $[M + Na]^+$: 617.17. Found: 617.17.

H_3DPASAm. Compound **2** (0.2501 g, 0.4206 mmol) was dissolved in 6 M HCl (20 mL) and the mixture was heated at 55 °C for 16 h. The acid was evaporated, water (3 mL) was added and evaporated again twice to remove most of the HCl. The ligand was isolated by filtration as a white solid (0.1435 g, 0.2528 mmol, 60% yield). ^1H NMR (500 MHz, D_2O, pH 14) δ 7.50−7.65 (m, 8H), 7.18 (m, 2H), 3.60 (s, 4H), 2.63 (m, 2H), 2.33 (m, 2H). ^{19}F NMR (376 MHz, D_2O, pH 14) δ −62.5. ^{13}C NMR (126 MHz, D_2O, pH 14) δ 172.7, 168.4, 157.6, 152.5, 146.5, 138.1, 126.5, 125.7, 125.3, 122.2, 60.0, 55.6, 42.2. HRMS (ESI^-): *m*/*z* calcd for $C_{23}H_{20}F_3N_4O_6S$ $[M-H]^-$: 537.1061. Found: 537.1064. Elemental analysis: calculated for $C_{23}H_{21}F_3N_4O_6S$·0.8HCl: C: 48.84; H: 3.69; N: 9.54. Found: C: 48.66; H: 3.87; N: 9.87. IR (ATR, ν[cm^{-1}]): 1738 ν(C═O), 1575 ν(C═N), 1356, 1322, 1164 ν(S═O).

***N*-(2-Bromoethyl)-4-(trifluoromethyl)benzenesulfonamide (3).** The synthesis followed the procedure reported for closely related compounds.[53] 2-Bromoethan-1-amine hydrobromide (0.4702 g, 2.295 mmol, 1 equiv) and triethylamine (0.640 mL, 4.5918 mmol, 2 equiv) were dissolved in CH_2Cl_2 (15 mL). 4-(Trifluoromethyl)-benzenesulfonyl chloride (0.5614 g, 2.295 mmol, 1 equiv) dissolved in CH_2Cl_2 (2 mL) was added dropwise to the solution while stirring at room temperature. The yellowish solution was stirred for 24 h. The solution was washed with 1 M HCl (3 × 15 mL) followed by brine (10 mL). The organic layer was dried using Na_2SO_4, filtered and the solvent was evaporated. The white solid was washed with acidified water (pH 5; 2 × 10 mL) and dried (0.6154 g, 1.853 mmol, 81% yield). ^1H NMR (300 MHz, $CDCl_3$): δ 8.02 (d, ^3J = 8.5 Hz, 2H), 7.81 (d, ^3J = 8.5 Hz, 2H), 5.24 (b, 1H), 3.43 (m, 4H). ^{19}F NMR (282 MHz, $CDCl_3$): −63.1. ^{13}C NMR (75.5 MHz, $CDCl_3$): δ 143.5, 127.5, 126.5 ($^2J_{C-F}$ = 3.8 Hz), 44.6, 31.5. MS (EI, 70 eV): *m*/*z* calcd for $C_9H_9BrF_3NO_2S$ $[M^+]$: 330.9. Found: 330.9. Elemental analysis: Calculated for $C_9H_9BrF_3NO_2S$: C: 32.55; H: 2.73; N: 4.22; S: 9.65. Found: C: 33.07; H: 2.62; N: 3.93; S: 9.54.

2,2′-(7-(2-((4-(Trifluoromethyl)phenyl) sulfonamido)ethyl)-1,4,7-triazonane-1,4-diyl)diacetate (4). Di-*tert*-Butyl 2,2′-(1,4,7-triazacyclononane-1,4-diyl)diacetate (0.1999 g, 0.5592 mmol, 1 equiv) was dissolved in dry CH_3CN (10 mL) and K_2CO_3 (0.1932 g, 1.398 mmol) was added under argon. The mixture was stirred at room temperature and compound **3** (0.1857 g, 0.5591 mmol, 1 equiv)

https://dx.doi.org/10.1021/acs.inorgchem.0c02098
Inorg. Chem. XXXX, XXX, XXX−XXX

dissolved in CH_3CN (5 mL) was added. The mixture was heated and stirred at 60 °C 24 h and then the carbonate was removed by filtration. The evaporation of the solvent yielded a yellowish oil that was purified on neutral alumina using MPLC (CH_2Cl_2/MeOH (10%)). The fractions containing the product were concentrated affording a yellow oil (0.3297 g, 0.5416 mmol, 97% yield). ^{1}H NMR (300 MHz, $CDCl_3$) δ 8.00 (d, ^3J = 8.3 Hz, 2H), 7.75 (d, ^3J = 8.3 Hz, 2H), 3.31 (s, 4H), 3.02 (t, ^3J = 5.4 Hz, 2H), 2.87−2.59 (m, 14H), 1.44 (s, 18H). ^{19}F NMR (282 MHz, $CDCl_3$): δ −63.0. ^{13}C NMR (126 MHz, $CDCl_3$): 171.3, 144.4, 133.8 (^1J = 32.9 Hz), 127.5, 126.0 (^2J = 3.6 Hz), 80.9, 58.9, 56.0, 55.3, 55.0, 54.7, 28.2. HRMS (ESI$^+$): m/z Calcd for $C_{27}H_{44}F_3N_4O_6S$ $[M + H]^+$: 609.2928. Found: 609.2916. IR (ATR, ν[cm^{-1}]): 1733 ν(C═O), 1323, 1159, 1129 ν(S═O).

H_3NO2ASAm. Compound **4** (0.1240 g, 0.2037 mmol) was dissolved in 3 M HCl (20 mL) and the mixture was stirred 24 h at room temperature. The acid was evaporated, water (3 mL) was added and evaporated again twice to remove most of the HCl. The product was lyophilized to afford a white solid (0.1096 g, 0.1838 mmol, 90% yield). ^{1}H NMR (500 MHz, D_2O, pH 1.5): 8.07 (d, ^3J = 8.3 Hz, 2H), 7.99 (d, ^3J = 8.3 Hz, 2H), 3.83 (s, 4H), 3.53−3.30 (m, 12H), 3.18 (s, 4H). ^{19}F NMR (282 MHz, D_2O, pH 1.5): δ −63.1. ^{13}C NMR (126 MHz, D_2O, pH 1.5): 173.9, 140.8, 134.5 ($^1J_{C-F}$ = 32.7 Hz), 127.6, 126.9 ($^2J_{C-F}$ = 3.7 Hz), 56.4, 55.4, 51.1, 49.9, 48.5, 38.3. HRMS (ESI$^+$): m/z calcd for $C_{19}H_{28}F_3N_4O_6S$ $[M + H]^+$: 497.1676. Found: 497.1668. Elemental analysis: Calculated for $C_{19}H_{27}F_3N_4O_6S{\cdot}2HCl{\cdot}1.5H_2O$: C: 38.26; H: 5.41; N: 9.39; S: 5.38. Found: C: 38.38; H: 5.14; N: 9.03; S: 5.03. IR (ATR, ν[cm^{-1}]): 1732 ν(C═O), 1321, 1163 ν(S═O).

Potentiometric and Spectrophotometric Measurements. Ligand protonation constants and stability and protonation constants of the Mn^{2+} complexes were determined by potentiometric or spectrophotometric titrations, using the HYPERQUAD2013 program.[54] All measurements were performed at 298 K with an ionic strength adjusted to 0.15 M using NaCl. Stability constants of the metal complexes were obtained from titrations at a metal-to-ligand concentration ratio of 1:1. The $MnCl_2$ solution was standardized by titration with EDTA at pH 10 (NH_3/NH_4Cl buffer) in the presence of triethanolamine to avoid manganese precipitation. Eriochrome Black T was employed as an indicator.[55] The concentration of the solution was double-checked by titrating chloride with $AgNO_3$, using potassium chromate as an indicator.[55]

Potentiometric titrations were performed with a dual-wall cell thermostated at 298 K using circulating water. All measurements were performed with magnetic stirring to homogenize the solutions (starting volume of 10 mL), while bubbling nitrogen on the surface of the solution to avoid CO_2 absorption. The concentration of the ligand in the titration cell was 2−3 mM, while titrations covered the pH range of ca. 2.0 to 12.0. The solution of the ligand, in the absence and presence of the metal ion, was titrated with standard solutions of hydrochloric acid or sodium hydroxide. The titrant was delivered with a Crison microBu 2030 automatic buret, using 2.5 or 1.0 mL syringes. A Crison micropH 2000 pH meter, connected to a glass electrode (Radiometer pHG211) and a reference electrode (Radiometer REF201), was used to measure the electromotive force (emf) values. The procedures used for electrode calibration were described in detail elsewhere.[56] The formation of the Mn^{2+} complexes of $DPASAm^{3-}$ and $NO2ASAm^{3-}$ was fast. In the case of the $NOTA^{3-}$ complex, the equilibrium was attained more slowly, taking 5−10 min, depending on the pH. Back titrations were performed to confirm that the equilibrium was attained.

The UV−vis absorption spectra were recorded with a Uvikon-XS (Bio-Tek Instruments) double-beam spectrophotometer, using cells with a path length of 1 cm. The spectra were recorded in the range 230−310 nm (80 wavelengths) for every solution. The pH of the solutions below 2.8 or above 11.9 was adjusted directly with standard solutions of hydrochloric acid or sodium hydroxide. Otherwise, different buffers were used to facilitate pH adjustment: borax, 0.0125 M (pH range 8−10.8); phosphate (pH ranges of 5.8−8.0, 0.05 M; and 10.9−12.0, 0.025 M) or acetate (pH range of 3.5−5.3, 0.02 M).[57] The HypSpec2014 program was used to determine the equilibrium constants and the spectra of the absorbing species.[54]

Relaxometric Measurements. $1/T_1$ ^{1}H nuclear magnetic relaxation dispersion (NMRD) profiles were measured with a fast-field cycling (FFC) Stelar SmarTracer relaxometer over a continuum of magnetic field strengths from proton Larmor frequencies of 0.01−10 MHz, with an uncertainty in $1/T_1$ of ca. 1%. Data in the 20−120 MHz range were collected with a high-field relaxometer (Stelar) that was equipped with the HTS-110 3T metrology cryogen-free superconducting magnet. The analyses were performed by using the standard inversion recovery sequence with a typical 90° pulse width of 3.5 μs and the reproducibility of the data was within ±0.5%. The temperature was controlled with a Stelar VTC-91 heater airflow equipped with a copper-constantan thermocouple (uncertainty of ±0.1 K).

The Mn^{2+} complexes were prepared by mixing solutions of $MnCl_2$ and the corresponding ligand, using a ∼5% molar excess of the latter to avoid the presence of free Mn^{2+} in solution. The pH was adjusted to ∼7.0 with HCl or NaOH. The concentration of Mn^{2+} chelates was assessed by ^{1}H NMR measurements (Bruker Advance III Spectrometer equipped with a wide-bore 11.7 T magnet), using the well-established Evans' method.[58]

Table 4. Crystal Data and Structure Refinement Details

parameter	value
formula	$C_{23}H_{26}F_3MnN_4NaO_{10}S$
molecular weight, MW	685.47
crystal system	triclinic
space group	$P\bar{1}$
a	8.9108(6) Å
b	9.2961(7) Å
c	17.0716(12) Å
α	97.133(2)°,
β	95.201(3)°
γ	97.178(2)°
V	1384.08(17) Å^3
F(000)	702
Z	2
D_{calc}	1.645 g cm^{-3}
μ	5.494 mm^{-1}
θ range	4.84°−71.28°
R_{int}	0.0485
measured reflections	22598[a]
goodness of fit, GOF on F^2	1.045
$R1$	0.0401
$wR2$ (all data)	0.1036
largest differences	0.504 e Å^{-3} (peak), −0.509 eÅ^{-3} (hole)

[a]Of which 5243 were independent and 5047 were unique, with $I > 2\sigma(I)$.

X-ray Diffraction Measurements. A single crystal of Na[Mn(DPASAm)(H_2O)]·2H_2O was analyzed via XRD. Crystallographic data were collected at room temperature using a Bruker Smart 6000 CCD detector and Cu Kα radiation (λ = 1.54178 Å) generated by an Incoatec microfocus source equipped with Incoatec Quazar MX optics. The software APEX2[59] was used for collecting frames of data, indexing reflections, and the determination of lattice parameters, SAINT[60] for integration of the intensity of reflections, and SADABS[61] for scaling and empirical absorption correction. The structure was solved by dual-space methods using the program SHELXT.[62] All non-hydrogen atoms were refined with anisotropic thermal parameters by full-matrix least-squares calculations on F^2 with the SHELXL-2018/3 program.[63] Hydrogen atoms were inserted at calculated positions and constrained with isotropic thermal parameters, except for the H atom of the water molecules, which were located from a Fourier-difference

https://dx.doi.org/10.1021/acs.inorgchem.0c02098
Inorg. Chem. XXXX, XXX, XXX−XXX

map and refined isotropically. Crystal data and structure refinement details are given in Table 4.

■ ASSOCIATED CONTENT

Supporting Information

The Supporting Information is available free of charge at https://pubs.acs.org/doi/10.1021/acs.inorgchem.0c02098.

Potentiometric titration curves, speciation diagrams, spectrophotometric titrations, relaxometric data, NMR and MS of ligands and their precursors (PDF)

Accession Codes

CCDC 2015848 contains the supplementary crystallographic data for this paper. These data can be obtained free of charge via www.ccdc.cam.ac.uk/data_request/cif, or by emailing data_request@ccdc.cam.ac.uk, or by contacting The Cambridge Crystallographic Data Centre, 12 Union Road, Cambridge CB2 1EZ, UK; fax: + 44 1223 336033.

■ AUTHOR INFORMATION

Corresponding Authors

Carlos Platas-Iglesias − *Centro de Investigacións Científicas Avanzadas (CICA) and Departamento de Química Fundamental, Universidade da Coruña, 15008 A Coruña, Spain;* orcid.org/0000-0002-6989-9654; Email: carlos.platas.iglesias@udc.es

Mauro Botta − *Dipartimento di Scienze e Innovazione Tecnologica, Università del Piemonte Orientale "A. Avogadro", 15121 Alessandria, Italy;* orcid.org/0000-0003-4192-355X; Email: mauro.botta@uniupo.it

Authors

Rocío Uzal-Varela − *Centro de Investigacións Científicas Avanzadas (CICA) and Departamento de Química Fundamental, Universidade da Coruña, 15008 A Coruña, Spain*

Aurora Rodríguez-Rodríguez − *Centro de Investigacións Científicas Avanzadas (CICA) and Departamento de Química Fundamental, Universidade da Coruña, 15008 A Coruña, Spain;* orcid.org/0000-0002-4951-4470

Miguel Martínez-Calvo − *Centro de Investigacións Científicas Avanzadas (CICA) and Departamento de Química Fundamental, Universidade da Coruña, 15008 A Coruña, Spain;* orcid.org/0000-0001-7059-0956

Fabio Carniato − *Dipartimento di Scienze e Innovazione Tecnologica, Università del Piemonte Orientale "A. Avogadro", 15121 Alessandria, Italy;* orcid.org/0000-0002-6268-1687

Daniela Lalli − *Dipartimento di Scienze e Innovazione Tecnologica, Università del Piemonte Orientale "A. Avogadro", 15121 Alessandria, Italy*

David Esteban-Gómez − *Centro de Investigacións Científicas Avanzadas (CICA) and Departamento de Química Fundamental, Universidade da Coruña, 15008 A Coruña, Spain;* orcid.org/0000-0001-6270-1660

Isabel Brandariz − *Centro de Investigacións Científicas Avanzadas (CICA) and Departamento de Química Fundamental, Universidade da Coruña, 15008 A Coruña, Spain*

Paulo Pérez-Lourido − *Departamento de Química Inorgánica, Facultad de Ciencias, Universidade de Vigo, 36310 Pontevedra, Spain;* orcid.org/0000-0003-2281-3064

Complete contact information is available at: https://pubs.acs.org/10.1021/acs.inorgchem.0c02098

Author Contributions

The manuscript was written through contributions of all authors. All authors have given approval to the final version of the manuscript.

Notes

The authors declare no competing financial interest.

■ ACKNOWLEDGMENTS

Authors C.P.-I. and D.E.-G. thank Ministerio de Economía y Competitividad (No. CTQ2016-76756-P) and Xunta de Galicia (Nos. ED431B 2017/59 and ED431D 2017/01) for generous financial support. R.U.-V. thanks Xunta de Galicia (No. ED481A-2018/314) for funding her Ph.D. contract. M.B., F.C., and D.L. are grateful to Università del Piemonte Orientale per financial support (No. FARC 2019). M.M.-C. thanks Ministerio de Ciencia e Innovación and Ministerio de Universidades for the Distinguished Research Contract "Beatriz Galindo" (No. BEAGAL18/00144).

■ REFERENCES

(1) Wahsner, J.; Gale, E. M.; Rodríguez-Rodríguez, A.; Caravan, P. Chemistry of MRI Contrast Agents: Current Challenges and New Frontiers. *Chem. Rev.* **2019**, *119*, 957−1057.

(2) *The Chemistry of Contrast Agents in Medical Magnetic Resonance Imaging*, 2nd Edition; Merbach, A., Helm, L., Tóth, É., Eds.; Wiley, 2013.

(3) Lauterbur, P. C.; Mendoça-Dias, M. H.; Rudin, A. A. Augmentation of Tissue Water Proton Spin-Lattice Relaxation Rates by In Vivo Addition of Paramagnetic Ions, in *Frontiers of Biological Energetics*; Dutton, P. O., Leigh, J., Scarpa, A., Eds.; Academic Press: New York, 1978; pp 752−759.

(4) Brady, T. J.; Gebhardt, M. C.; Pykett, I. L.; Buonanno, F. S.; Newhouse, J. H.; Burt, C. T.; Smith, R. J.; Mankin, H. J.; Kistler, J. P.; Goldman, M. R.; Hinshaw, W. S.; Pohost, G. M. NMR Imaging of Forearms in Healthy Volunteers and Patients with Giant-Cell Tumor of Bone. *Radiology* **1982**, *144*, 549−552.

(5) Goldman, M. R.; Brady, T. J.; Pykett, I. L.; Burt, C. T.; Buonanno, F. S.; Kistler, J. P.; Newhouse, J. H.; Hinshaw, W. S.; Pohost, G. M. Quantification of Experimental Myocardial Infarction Using Nuclear Magnetic Resonance Imaging and Paramagnetic Ion Contrast Enhancement in Excised Canine Hearts. *Circulation* **1982**, *66*, 1012−1016.

(6) Young, I. R.; Clarke, G. J.; Baffles, D. R.; Pennock, J. M.; Doyle, F. H.; Bydder, G. M. Enhancement of Relaxation Rate with Paramagnetic Contrast Agents in NMR Imaging. *Clin. Imag.* **1981**, *5*, 543−547.

(7) Carr, D. H.; Brown, J.; Bydder, G. M.; Weinmann, H. J.; Speck, U.; Thomas, D. J.; Young, I. R. Intravenous Chelated Gadolinium as a Contrast Agent in NMR Imaging of Cerebral Tumours. *Lancet* **1984**, *323*, 484−486.

(8) Sarka, L.; Burai, L.; Brücher, E. The Rates of the Exchange Reactions between $[Gd(DTPA)]^{2-}$ and the Endogenous Ions Cu^{2+} and Zn^{2+}: A Kinetic Model for the Prediction of the In Vivo Stability of $[Gd(DTPA)]^{2-}$, Used as a Contrast Agent in Magnetic Resonance Imaging. *Chem. - Eur. J.* **2000**, *6*, 719−724.

(9) Sherry, A. D.; Wu, Y. The Importance of Water Exchange Rates in the Design of Responsive Agents for MRI. *Curr. Opin. Chem. Biol.* **2013**, *17*, 167−174.

(10) Grobner, T. Gadolinium - A Specific Trigger for the Development of Nephrogenic Fibrosing Dermopathy and Nephrogenic Systemic Fibrosis? *Nephrol., Dial., Transplant.* **2006**, *21*, 1104−1108.

(11) Marckmann, P.; Skov, L.; Rossen, K.; Dupont, A.; Damholt, M. B.; Heaf, J. G.; Thomsen, H. S. Nephrogenic Systemic Fibrosis: Suspected Causative Role of Gadodiamide Used for Contrast-Enhanced Magnetic Resonance Imaging. *J. Am. Soc. Nephrol.* **2006**, *17*, 2359−2362.

(12) (a) Kanal, E.; Tweedle, M. F. Residual or Retained Gadolinium: Practical Implications for Radiologists and Our Patients. *Radiology* **2015**, *275*, 630−634. (b) Fraum, T. J.; Ludwig, D. R.; Bashir, M. R.; Fowler, K. J. Gadolinium-Based Contrast Agents: A Comprehensive Risk Assessment. *J. Magn. Reson. Imaging* **2017**, *46*, 338−353.
(13) Le Fur, M.; Caravan, P. The Biological Fate of Gadolinium-Based MRI Contrast Agents: A Call to Action for Bioinorganic Chemists. *Metallomics* **2019**, *11*, 240−254.
(14) Viswanathan, S.; Kovacs, Z.; Green, K. N.; Ratnakar, S. J.; Sherry, A. D. Alternatives to Gadolinium-Based Metal Chelates for Magnetic Resonance Imaging. *Chem. Rev.* **2010**, *110*, 2960−3018.
(15) (a) Gupta, A.; Caravan, P.; Price, W. S.; Platas-Iglesias, C.; Gale, E. M. Applications for Transition-Metal Chemistry in Contrast-Enhanced Magnetic Resonance Imaging. *Inorg. Chem.* **2020**, *59*, 6648−6678. (b) Drahos, B.; Lukes, I.; Toth, E. Manganese(II) Complexes as Potential Contrast Agents for MRI. *Eur. J. Inorg. Chem.* **2012**, *2012*, 1975−1986. (c) Pan, D.; Schmieder, A. H.; Wickline, S. A.; Lanza, G. M. Manganese-Based MRI Contrast Agents: Past, Present, and Future. *Tetrahedron* **2011**, *67*, 8431−8444.
(16) (a) Gale, E. M.; Atanasova, I. P.; Blasi, F.; Ay, I.; Caravan, P. A Manganese Alternative to Gadolinium for MRI Contrast. *J. Am. Chem. Soc.* **2015**, *137*, 15548−15557. (b) Rolla, G. A.; Platas-Iglesias, C.; Botta, M.; Tei, L.; Helm, L. ^{1}H and ^{17}O NMR Relaxometric and Computational Study on Macrocyclic Mn(II) Complexes. *Inorg. Chem.* **2013**, *52*, 3268−3279. (c) Su, H.; Wu, C.; Zhu, J.; Miao, T.; Wang, D.; Xia, C.; Zhao, X.; Gong, Q.; Song, B.; Ai, H. Rigid Mn(II) Chelate as Efficient MRI Contrast Agent for Vascular Imaging. *Dalton Trans.* **2012**, *41*, 14480−14483. (d) Phukan, B.; Mukherjee, C.; Goswami, U.; Sarmah, A.; Mukherjee, S.; Sahoo, S. K.; Moi, S. C. A New Bis(aquated) High Relaxivity Mn(II) Complex as an Alternative to Gd(III)-Based MRI Contrast Agent. *Inorg. Chem.* **2018**, *57*, 2631−2638. (e) Ndiaye, D.; Sy, M.; Pallier, A.; Même, S.; de Silva, I.; Lacerda, S.; Nonat, A. M.; Charbonnière, L. J.; Tóth, É. Unprecedented Kinetic Inertness for a Mn^{2+}-Bispidine Chelate: A Novel Structural Entry for Mn^{2+}-Based Imaging Agents. *Angew. Chem., Int. Ed.* **2020**, *59*, 11958−11963.
(17) (a) Rodríguez, E.; Roig, A.; Molins, E.; Arús, C.; Quintero, M. R.; Cabañas, M. E.; Cerdán, S.; Lopez-Larrubia, P.; Sanfeliu, C. In vitro Characterization of an Fe_8 Cluster as Potential MRI Contrast Agent. *NMR Biomed.* **2005**, *18*, 300−307. (b) Wang, H.; Jordan, V. C.; Ramsay, I. A.; Sojoodi, M.; Fuchs, B. C.; Tanabe, K. K.; Caravan, P.; Gale, E. M. Molecular Magnetic Resonance Imaging Using a Redox-Active Iron Complex. *J. Am. Chem. Soc.* **2019**, *141*, 5916−5925.
(18) Lux, J.; Sherry, A. D. Advances in Gadolinium-Based MRI Contrast Agent Designs for Monitoring Biological Processes in vivo. *Curr. Opin. Chem. Biol.* **2018**, *45*, 121−130.
(19) Angelovski, G. What We Can Really Do with Bioresponsive MRI Contrast Agents. *Angew. Chem., Int. Ed.* **2016**, *55*, 7038−7046.
(20) Heffern, M. C.; Matosziuk, L. M.; Meade, T. J. Lanthanide Probes for Bioresponsive Imaging. *Chem. Rev.* **2014**, *114*, 4496−4539.
(21) Botár, R.; Molnár, E.; Trencsényi, G.; Kiss, J.; Kálmán, F. K.; Tircsó, G. Stable and Inert Mn(II)-Based and pH-Responsive Contrast Agents. *J. Am. Chem. Soc.* **2020**, *142*, 1662−1666.
(22) Forgacs, A.; Pujales-Paradela, R.; Regueiro-Figueroa, M.; Valencia, L.; Esteban-Gomez, D.; Botta, M.; Platas-Iglesias, C. Developing the Family of Picolinate Ligands for Mn^{2+} Complexation. *Dalton Trans.* **2017**, *46*, 1546−1558.
(23) (a) Regueiro-Figueroa, M.; Rolla, G. A.; Esteban-Gómez, D.; de Blas, A.; Rodriguez-Blas, T.; Botta, M.; Platas-Iglesias, C. High Relaxivity Mn^{2+}-Based MRI Contrast Agents. *Chem. - Eur. J.* **2014**, *20*, 17300−17305. (b) Forgacs, A.; Regueiro-Figueroa, M.; Barriada, J. L.; Esteban-Gomez, D.; de Blas, A.; Rodriguez-Blas, T.; Botta, M.; Platas-Iglesias, C. Mono-, Bi-, and Trinuclear Bis-Hydrated Mn^{2+} Complexes as Potential MRI Contrast Agents. *Inorg. Chem.* **2015**, *54*, 9576−9587.
(24) Molnar, E.; Camus, N.; Patinec, V.; Rolla, G. A.; Botta, M.; Tircso, G.; Kalman, F. K.; Fodor, T.; Tripier, R.; Platas-Iglesias, C. Picolinate-Containing Macrocyclic Mn^{2+} Complexes as Potential MRI Contrast Agents. *Inorg. Chem.* **2014**, *53*, 5136−5149.
(25) (a) Pujales-Paradela, R.; Carniato, F.; Esteban-Gomez, D.; Botta, M.; Platas-Iglesias, C. Controlling water exchange rates in potential Mn^{2+}-based MRI agents derived from $NO2A^{2-}$. *Dalton Trans.* **2019**, *48*, 3962−3972. (b) Patinec, V.; Rolla, G. A.; Botta, M.; Tripier, R.; Esteban-Gomez, D.; Platas-Iglesias, C. Hyperfine Coupling Constants on Inner-Sphere Water Molecules of a Triazacyclononane-based Mn(II) Complex and Related Systems Relevant as MRI Contrast Agents. *Inorg. Chem.* **2013**, *52*, 11173−11184.
(26) Forgács, A.; Tei, L.; Baranyai, Z.; Esteban-Gómez, D.; Platas-Iglesias, C.; Botta, M. Optimising the relaxivities of Mn^{2+} complexes by targeting human serum albumin (HSA). *Dalton Trans.* **2017**, *46*, 8494−8504.
(27) (a) Lowe, M. P.; Parker, D.; Reany, O.; Aime, S.; Botta, M.; Castellano, G.; Gianolio, E.; Pagliarin, R. pH-Dependent Modulation of Relaxivity and Luminescence in Macrocyclic Gadolinium and Europium Complexes Based on Reversible Intramolecular Sulfonamide Ligation. *J. Am. Chem. Soc.* **2001**, *123*, 7601−7609. (b) Lowe, M. P.; Parker, D. Controllable pH Modulation of Lanthanide Luminescence by Intramolecular Switching of the Hydration State. *Chem. Commun.* **2000**, 707−708. (c) Takács, A.; Napolitano, R.; Purgel, M.; Bényei, A. C.; Zékány, L.; Brücher, E.; Tóth, I.; Baranyai, Z.; Aime, S. Solution Structures, Stabilities, Kinetics, and Dynamics of DO3A and DO3A−Sulphonamide Complexes. *Inorg. Chem.* **2014**, *53*, 2858−2872. (d) Moriggi, L.; Yaseen, M. A.; Helm, L.; Caravan, P. Serum Albumin Targeted, pH-Dependent Magnetic Resonance Relaxation Agents. *Chem. - Eur. J.* **2012**, *18*, 3675−3686.
(28) (a) Casanova, D.; Alemany, P.; Bofill, J. M.; Alvarez, S. Shape and Symmetry of Heptacoordinate Transition-Metal Complexes: Structural Trends. *Chem. - Eur. J.* **2003**, *9*, 1281−1295. (b) Regueiro-Figueroa, M.; Lima, L. M. P.; Blanco, V.; Esteban-Gómez, D.; de Blas, A.; Rodríguez-Blas, T.; Delgado, R.; Platas-Iglesias, C. Reasons Behind the Relative Abundances of Heptacoordinate Complexes along the Late First-Row Transition Metal Series. *Inorg. Chem.* **2014**, *53*, 12859−12869.
(29) (a) Huang, Q.; Zhai, B. Crystal Structure, Thermal and Magnetic Studies of a Dinuclear Mn(II) Complex with Decadentate Picolinate Based Ligand. *J. Coord. Chem.* **2007**, *60*, 2257−2263. (b) Khannam, M.; Weyhermüller, T.; Goswami, U.; Mukherjee, C. A Highly Stable L-Alanine-Based Mono(aquated) Mn(II) Complex as a T_1-Weighted MRI Contrast Agent. *Dalton Trans.* **2017**, *46*, 10426−10432. (c) Gerey, B.; Gennari, M.; Gouré, E.; Pécaut, J.; Blackman, A.; Pantazis, D.; Neese, F.; Molton, F.; Fortage, J.; Duboc, C.; Collomb, M.-N. Calcium and Heterometallic Manganese−Calcium Complexes Supported by Tripodal Pyridinecarboxylate Ligands: Structural, EPR and Theoretical Investigations. *Dalton Trans.* **2015**, *44*, 12757−12770. (d) Martin-Diaconescu, V.; Gennari, M.; Gerey, B.; Tsui, E.; Kanady, J.; Tran, R.; Pecaut, J.; Maganas, D.; Krewald, V.; Goure, E.; Duboc, C.; Yano, J.; Agapie, T.; Collomb, M.-N.; DeBeer, S. Ca K-Edge XAS as a Probe of Calcium Centers in Complex Systems. *Inorg. Chem.* **2015**, *54*, 1283−1292.
(30) (a) Macías, B.; Villa, M. V.; Lapresa, R.; Alzuet, G.; Hernández-Gil, J.; Sanz, F. Mn(II) Complexes with Sulfonamides as Ligands. DNA Interaction Studies and Nuclease Activity. *J. Inorg. Biochem.* **2012**, *115*, 64−71. (b) Seidler-Egdal, R. K.; Johansson, F. B.; Veltze, S.; Skou, E. M.; Bond, A. D.; McKenzie, C. J. Tunability of the $M^{II}M^{III}/M^{II}_2$ and $M^{III}_2/M^{II}M^{III}$ (M = Mn, Co) Couples in bis-μ-*O*,*Ó*-Carboxylato-μ-OR Bridged Complexes. *Dalton Trans.* **2011**, *40*, 3336−3345. (c) Veltze, S.; Egdal, R. K.; Johansson, F. B.; Bond, A. D.; McKenzie, C. J. Coordinative Fexibility in an Acyclic Bis-(sulfonamide) Ligand. *Dalton Trans.* **2009**, 10495−10504.
(31) Gao, J.; Ye, K.; He, M.; Xiong, W.-W.; Cao, W.; Lee, Z. Y.; Wang, Y.; Wu, T.; Huo, F.; Liu, X.; Zhang, Q. Tuning Metal−Carboxylate Coordination in Crystalline Metal−Organic Frameworks Through Surfactant Media. *J. Solid State Chem.* **2013**, *206*, 27−31.

https://dx.doi.org/10.1021/acs.inorgchem.0c02098
Inorg. Chem. XXXX, XXX, XXX−XXX

(32) Drahos, B.; Kubicek, V.; Bonnet, C. S.; Hermann, P.; Lukes, I.; Toth, E. Dissociation Kinetics of Mn^{2+} Complexes of NOTA and DOTA. *Dalton Trans.* **2011**, *40*, 1945−1951.
(33) Van der Merwe, M. J.; Boeyens, J. C. A.; Hancock, R. D. Crystallographic and Thermodynamic Study of Metal Ion Size Selectivity in the Ligand 1,4,7-Triazacyclononane-*N*,*N*',*N*"-triacetate. *Inorg. Chem.* **1985**, *24*, 1208−1213.
(34) Pujales-Paradela, R.; Carniato, F.; Uzal-Varela, R.; Brandariz, I.; Iglesias, E.; Platas-Iglesias, C.; Botta, M.; Esteban-Gómez, D. A Pentadentate Member of the Picolinate Family for Mn(II) Complexation and an Amphiphilic Derivative. *Dalton Trans.* **2019**, *48*, 696−710.
(35) Takacs, A.; Napolitano, R.; Purgel, M.; Benyei, A. C.; Zekany, L.; Brucher, E.; Toth, I.; Baranyai, Z.; Aime, S. Solution Structures, Stabilities, Kinetics, and Dynamics of DO3A and DO3A−Sulphonamide Complexes. *Inorg. Chem.* **2014**, *53*, 2858−2872.
(36) Lowe, M. P.; Parker, D. pH Switched Sensitisation of Europium(III) by a Dansyl group. *Inorg. Chim. Acta* **2001**, *317*, 163−173.
(37) Rodríguez-Rodríguez, A.; Garda, Z.; Ruscsák, E.; Esteban-Gómez, D.; de Blas, A.; Rodríguez-Blas, T.; Lima, L. M. P.; Beyler, M.; Tripier, R.; Tircsó, G.; Platas-Iglesias, C. Stable Mn^{2+}, Cu^{2+} and Ln^{3+} Complexes with Cyclen-Based Ligands Functionalized with Picolinate Pendant Arms. *Dalton Trans.* **2015**, *44*, 5017−5031.
(38) Amendola, V.; Fabbrizzi, L.; Mosca, L.; Schmidtchen, F.-P. Urea-, Squaramide-, and Sulfonamide-Based Anion Receptors: A Thermodynamic Study. *Chem. - Eur. J.* **2011**, *17*, 5972−5981.
(39) Cortes, S.; Brucher, E.; Geraldes, C. F. G. C.; Sherry, A. D. Potentiometry and NMR Studies of l,5,9-Triazacyclododecane-N,N',N"-triacetic Acid and Its Metal Ion Complexes. *Inorg. Chem.* **1990**, *29*, 5−9.
(40) Drahos, B.; Kotek, J.; Hermann, P.; Lukes, I.; Toth, E. Mn^{2+} Complexes with Pyridine-Containing 15-Membered Macrocycles: Thermodynamic, Kinetic, Crystallographic, and $^{1}H/^{17}O$ Relaxation Studies. *Inorg. Chem.* **2010**, *49*, 3224−3238.
(41) Botta, M.; Carniato, F.; Esteban-Gómez, D.; Platas-Iglesias, C.; Tei, L. Mn(II) Compounds as an Alternative to Gd-Based MRI Probes. *Future Med. Chem.* **2019**, *11*, 1461−1483.
(42) Esteban-Gómez, D.; Cassino, C.; Botta, M.; Platas-Iglesias, C. ^{17}O and ^{1}H Relaxometric and DFT Study of Hyperfine Coupling Constants in $[Mn(H_2O)_6]^{2+}$. *RSC Adv.* **2014**, *4*, 7094−7103.
(43) Balogh, E.; He, Z.; Hsieh, W.; Liu, S.; Toth, E. Dinuclear Complexes Formed with the Triazacyclononane Derivative $ENOTA^{4-}$: High-Pressure ^{17}O NMR Evidence of an Associative Water Exchange on $[Mn^{II}_2(ENOTA)(H_2O)_2]$. *Inorg. Chem.* **2007**, *46*, 238−250.
(44) Aime, S.; Botta, M.; Esteban-Gómez, D.; Platas-Iglesias, C. Characterisation of Magnetic Resonance Imaging (MRI) Contrast Agents Using NMR Relaxometry. *Mol. Phys.* **2019**, *117*, 898−909.
(45) Freed, J. H. Dynamic Effects of Pair Correlation Functions on Spin Relaxation by Translational Diffusion in Liquids. II. Finite Jumps and Independent T_1 Processes. *J. Chem. Phys.* **1978**, *68*, 4034−4037.
(46) Mills, R. Self-Diffusion in Normal and Heavy Water in the Range 1−45°. *J. Phys. Chem.* **1973**, *77*, 685−688.
(47) Luz, Z.; Meiboom, S. Proton Relaxation in Dilute Solutions of Cobalt(II) and Nickel(II) Ions in Methanol and the Rate of Methanol Exchange of the Solvation Sphere. *J. Chem. Phys.* **1964**, *40*, 2686−2693.
(48) (a) Solomon, I. Relaxation Processes in a System of Two Spins. *Phys. Rev.* **1955**, *99*, 559−565. (b) Solomon, I.; Bloembergen, N. Nuclear Magnetic Interactions in the HF Molecule. *J. Chem. Phys.* **1956**, *25*, 261−266. (c) Bloembergen, N. Proton Relaxation Times in Paramagnetic Solutions. *J. Chem. Phys.* **1957**, *27*, 572−573. (d) Bloembergen, N.; Morgan, L. O. Proton Relaxation Times in Paramagnetic Solutions. Effects of Electron Spin Relaxation. *J. Chem. Phys.* **1961**, *34*, 842−850.
(49) Gale, E. M.; Zhu, J.; Caravan, P. Direct Measurement of the Mn(II) Hydration State in Metal Complexes and Metalloproteins through ^{17}O NMR Line Widths. *J. Am. Chem. Soc.* **2013**, *135*, 18600−18608.
(50) (a) Borel, A.; Kang, H.; Gateau, C.; Mazzanti, M.; Clarkson, R. B.; Belford, R. L. Variable Temperature and EPR Frequency Study of Two Aqueous Gd(III) Complexes with Unprecedented Sharp Lines. *J. Phys. Chem. A* **2006**, *110*, 12434−12438. (b) Borel, A.; Laus, S.; Ozarowski, A.; Gateau, C.; Nonat, A.; Mazzanti, M.; Helm, L. Multiple-Frequency EPR Spectra of Two Aqueous Gd^{3+} Polyamino Polypyridine Carboxylate Complexes: A Study of High Field Effects. *J. Phys. Chem. A* **2007**, *111*, 5399−5407. (c) Khan, S.; Kubica-Misztal, A.; Kruk, D.; Kowalewski, J.; Odelius, M. Systematic Theoretical Investigation of the Zero-Field Splitting in Gd(III) Complexes: Wave Function and Density Functional Approaches. *J. Chem. Phys.* **2015**, *142*, No. 034304.
(51) Fornasier, R.; Milani, D.; Scrimin, P.; Tonellato, U. Functional Micellar Catalysis. Part 8. Catalysis of the Hydrolysis of *p*-Nitrophenyl Picolinate by Metal-Chelating Micelles Containing Copper(II) or Zinc(II). *J. Chem. Soc., Perkin Trans. 2* **1986**, *2*, 233−237.
(52) Tan, J.; Tang, W.; Sun, Y.; Jiang, Z.; Chen, F.; Xu, L.; Fan, Q.; Xiao, J. pH-Regulated Transfer Hydrogenation of Quinoxalines with a Cp*Ir-diamine Catalyst in Aqueous Media. *Tetrahedron* **2011**, *67*, 6206−6213.
(53) Moss, T. A.; Barber, D. M.; Kyle, A. F.; Dixon, D. J. Catalytic Asymmetric Alkylation Reactions for the Construction of Protected Ethylene-Amino and Propylene-Amino Motifs Attached to Quaternary Sterocenters. *Chem. - Eur. J.* **2013**, *19*, 3071−3081.
(54) Gans, P.; Sabatini, A.; Vacca, A. Investigation of Equilibria in Solution. Determination of Equilibrium Constants with the HYPERQUAD Suite of Programs. *Talanta* **1996**, *43*, 1739−1753.
(55) Vogel, A. I. *Vogel's Textbook of Quantitative Chemical Analysis*; Longman Scientific & Technical, Wiley: Harlow, Essex, New York, 1989.
(56) Caneda-Martínez, L.; Valencia, L.; Fernández-Pérez, I.; Regueiro-Figueroa, M.; Angelovski, G.; Brandariz, I.; Esteban-Gómez, D.; Platas-Iglesias, C. Toward Inert Paramagnetic Ni(II)-Based Chemical Exchange Saturation Transfer MRI Agents. *Dalton Trans.* **2017**, *46*, 15095−15106.
(57) Bates, R. G.: *Determination of pH, Theory and Practice*. 2nd Edition; John Wiley & Sons: New York, London, Sydney, Toronto, 1973.
(58) (a) Evans, D. F. The Determination of the Paramagnetic Susceptibility of Substances in Solution by Nuclear Magnetic Resonance. *J. Chem. Soc.* **1959**, 2003−2005. (b) Evans, D. F.; Fazakerley, G. V.; Phillips, R. F. Organometallic Compounds of Bivalent Europium, Ytterbium, and Samarium. *J. Chem. Soc. A* **1971**, 1931−1934.
(59) *APEX2, SMART, SAINT*; Bruker AXS, Inc.: Madison, WI, USA, 2007.
(60) *SAINT, Version 8.37A*; Bruker AXS, Inc.: Madison, WI, USA, 2015.
(61) Sheldrick, G. M. *SADABS, Version 2014/5*; Bruker AXS, Inc.: Madison, WI, USA.
(62) (a) *SHELXT, Version 2014/5*. (b) Sheldrick, G. M. SHELXT - Integrated Space-Group and Crystal-Structure Determination. *Acta Crystallogr., Sect. A: Found. Adv.* **2015**, *A71*, 3−8.
(63) (a) *SHELXL, Version 2018/3*. (b) Sheldrick, G. M. A Short History of SHELX. *Acta Crystallogr., Sect. A: Found. Crystallogr.* **2008**, *A64*, 112−122.

https://dx.doi.org/10.1021/acs.inorgchem.0c02098
Inorg. Chem. XXXX, XXX, XXX−XXX